Bistatic SAR coherence improvement through spatially variant polarimetry

By Daniel Andre

Centre for Electronic Warfare, Cranfield University, Defence Academy of the United Kingdom, Shrivenham, UK.

Abstract

Synthetic Aperture Radar (SAR) Coherent Change Detection (CCD) and interferometry depend on high coherence between a pair of SAR images. In principle these approaches allow a sensitive change detection for example of vehicle tracks or due to ground subsidence, both applications having clear and important military and civilian benefits.

One coherence requirement is that an overlap of the image supports in the radar spatial frequency domain is required. Previously the author has shown that over mountainous terrain or in SAR-near field scenarios, one may enhance SAR image coherence through Spatially Variant Incoherence Trimming (SVIT). However, it is additionally recognized that variation in bistatic Radar Cross-Section (RCS) from the ground is a factor that can lead to a loss of coherence between bistatic SAR collections.

Here it is shown that to further improve SAR image coherence, bistatic polarimetric effects should be taken into account as they can lead to a significant change in RCS as a function of the changing bistatic geometry. Bistatic scattering in different polarimetric basis are calculated for a representative example scatterer over a full bistatic hemisphere of scattering geometries, indicating the receiver polarization necessary for maximising bistatic RCS and coherence.

The results indicate that for diffuse specular scattering ground, the bistatic polarimetric scattering response varies in a well-defined way, so that it is possible to develop an extension to previous SVIT techniques, varying the bistatic polarization decomposition in a spatially variant manner to increase SAR coherence over the scene. In order to accomplish this in the SAR-near-field or mountainous terrain scenario, within the bistatic back projection image formation algorithm the appropriate bistatic polarimetric decomposition should be chosen for each radar pulse in the SAR aperture and for each SAR image pixel. In general the appropriate basis will be different for the two SAR collections for which one wishes to improve coherence. For the flat ground and SAR-far-field scenario, both mono and bistatic, the optimal approach reduces to a simpler approach of enhancement by adding linear combinations of globally polarimetric decomposed whole SAR images.

Having shown the effect for specular scattering in the Physical Optics (PO) regime, it is recognized that there may be situations in which ground returns are dominated by other kinds of scatterers in different scattering regimes, and with other polarimetric basis for enhancement of bistatic coherence, and that these would then need to be investigated further.

1. Introduction and Motivation

Synthetic Aperture Radar (SAR) Coherent Change Detection (CCD) and interferometry depend on high coherence between a pair of SAR images. In principle these approaches allow a sensitive change detection for example due to vehicle tracks or due to ground subsidence, both applications having clear and important military and civilian benefits.

One coherence requirement for SAR CCD is that an overlap of the image supports in the radar spatial frequency domain is required. Previously the author has shown that over mountainous terrain or in SAR-near field scenarios, one may enhance SAR image coherence through Spatially Variant Incoherence Trimming (SVIT) of the spatial frequency (K-space) data, (see for example Blacknell, D, Andre, D & Finch, C., 2010 and both references Andre, D., Morrison, K. & Blacknell, D., 2013). However, it is additionally recognized that variation in bistatic Radar Cross-Section (RCS) from the ground is a factor that can lead to a loss of coherence between bistatic SAR collections, and this work begins to address this issue.

Monostatic radar geometries have transmitter and receiver co-located, whereas in bistatic geometries these have a significant separation. There is considerable current interest in applications of bistatic radar geometries, as these allow novel sensing modes and opportunities. For example bistatic SAR imaging using transmitters of opportunity, such as television and radar broadcasts. These sensing modes would be covert. In addition, stealth targets would generally be visible under bistatic modes, as these are generally designed for stealth in specific monostatic conditions (see Willis, N & Griffiths, H., 2007 for a review of bistatic radar applications).

Regarding ground CCD, in the same way that monostatic Synthetic Aperture Radar (SAR) images can be dominated by specular (reflective) backscattering, it may be that for some terrain, bistatic SAR images may be dominated by specular scattering from the transmitter to the receiver. It may be that in some areas, diffuse scattering responsible for

bright bistatic SAR image textures are dominated by specular bistatic scattering, for example from stony surfaces. In these situations it would be advantageous to maximise this stable ground signal for improved CCD.

This kind of diffuse specular scattering is simple to define geometrically, as it is defined by a scatterer tangent surface, where the surface normal bisects two chords: that connecting the transmitter and scattering point, and that connecting the receiver and scattering point. It is acknowledged that bistatic scattering other than specular scattering may dominate in other circumstances, however in this initial study the specular scattering behaviour is investigated in order to show that non-trivial polarimetric effects do appear in general bistatic SAR imagery.

For greatest coherence we are interested primarily in these brightest scattering events that may dominate bistatic SAR, and as these may happen everywhere over the scene, we will assume that they do indeed happen everywhere in the scene. We use this model as a basis to predict the bistatic radar polarizations which provide the greatest scene Radar Cross-Section (RCS) resulting from specular scattering. It is emphasized that there will be competing polarimetric responses from any given ground type, however it is thought likely that these "one-bounce" specular scattering events will be more stable under geometry variation, and the polarization will shift in a gradual and well defined way.

It is noted that when a second bistatic SAR image is collected and its geometry is different from the first bistatic SAR geometry, and where the underlying spatial frequency image supports overlap (a requirement for CCD), it is generally the case that the bistatic polarizations which capture the brightest specular scattering in each geometry may be different from each other, even though they may originate from almost the same individual scattering points, for example on individual stones. This will be made clear through the development of the model and an example geometry in Sections 2 and 3. Thus it is proposed that there may be a situation where there will be coherence between two different bistatic geometries, and the coherence is greatest when the bistatic SAR images are collected in two *different* polarizations, both associated with specular scattering.

For convenience, the "high frequency" physical optics regime is considered here, however similar calculations can be performed for scatterers in other physical scattering regimes, such as the Rayleigh "low frequency" regime, and in this situation, non-trivial polarimetric effects may also be present.

2. Mathematical Development of Specular Scattering Model

For a bistatic collection we define a transmitter position vector **T**, a receiver position vector **R** and a scatterer position vector **S**. Diffuse scattering is assumed to be present over the scene and in the first instance this is modelled as specular (reflective) scattering from a curved surface at reflection point **S**, with tangent plane normal **N**, which is the bisector of **T**-**S** and **R**-**S**. The unit vector associated with **T**-**S** is $\mathbf{U}_{TS} = (\mathbf{T}\text{-}\mathbf{S}) / |\mathbf{T}\text{-}\mathbf{S}|$ and similarly that for **R**-**S** is $\mathbf{U}_{RS} = (\mathbf{R}\text{-}\mathbf{S})/|\mathbf{R}\text{-}\mathbf{S}|$. Hence the equation for **N** is:

$$\mathbf{N} = (\mathbf{U}_{TS} + \mathbf{U}_{RS}) / |\mathbf{U}_{TS} + \mathbf{U}_{RS}| \qquad (2.1)$$

With the Normal vector defined, it is now possible to define the specular scattering transformation matrix **M**:

$$\mathbf{M} = \mathbf{I} - 2\,\mathbf{N}\,\mathbf{N}^{T} = \mathbf{I} - 2\,\mathbf{P}_{N} \qquad (2.2)$$

Where "**I**" is the three by three identity matrix and $\mathbf{N}\,\mathbf{N}^{T}$ is a three by three projector onto **N**, denoted by $\mathbf{P}_N$.
M transforms the incident ray direction $\mathbf{K}_I$ into the specularly scattered direction $\mathbf{K}_S$:

$$\mathbf{K}_S = \mathbf{M}\,\mathbf{K}_I \qquad (2.3)$$

In addition to this however, **M** also transforms the incident electric field vector associated with the incident plane wave $\mathbf{E}_I$ to the scattered electric field vector associated with the scattered plane wave ES (see Ulaby, F. & Elachi, C., 1990, equation 3.46):

$$\mathbf{E}_S = \mathbf{M}\,\mathbf{E}_I \qquad (2.4)$$

It can be seen that where incident polarizations are linear, then specularly scattered polarizations are also linear. N.B. the overall magnitude of the electric field is also modified, but it is expected that this will occur in a similar way over the whole scene.

By definitions, it is the case that if $\mathbf{H}_T$ and $\mathbf{V}_T$ are the transmitter polarization basis vectors and $\mathbf{H}_R$ and $\mathbf{V}_R$ are the receiver polarization vectors, then the bistatic polarization components are:

$$\begin{aligned} HH &= \mathbf{H}_R^T \mathbf{M} \mathbf{H}_T & HV &= \mathbf{V}_R^T \mathbf{M} \mathbf{H}_T \\ VH &= \mathbf{H}_R^T \mathbf{M} \mathbf{V}_T & VV &= \mathbf{V}_R^T \mathbf{M} \mathbf{V}_T \end{aligned} \qquad (2.5)$$

Because the scattering mechanism is restricted to be the special case where there is bistatic specular reflection, **M** is a symmetric three-by-three matrix and this implies that:

$$HH = VV \quad \text{and} \quad HV = VH \qquad (2.6)$$

In general, bistatic scattering is well known for being non-reciprocal, however for bistatic specular scattering it is symmetric. The above result also has simplifying implications for polarization represented in other basis, such as the circular polarization basis. In this case the basis vectors **l** and **r** are (see Ulaby, F. & Elachi, C., 1990):

$$\mathbf{l} = \mathbf{h} + i\,\mathbf{v} \quad \text{and} \quad \mathbf{r} = \mathbf{h} - i\,\mathbf{v} \qquad (2.7)$$

and utilizing the linear polarization symmetries above it can be shown that:

$$LL = i\,HV, \quad RR = -i\,HV, \quad LR = HH, \quad RL = HH \qquad (2.8)$$

It is emphasized that although these simple outcomes hold for the symmetry involved in the simple bistatic specular reflection case, they would not hold in general.

Hence for bistatic specular scattering we expect:

$$|HH| = |VV| = |LR| = |RL| \quad \text{and} \quad |HV| = |VH| = |RR| = |LL| \qquad (2.9)$$

As noted previously, here we are interested in the far-field physical optics high frequency bistatic scattering case. In this scenario it is useful to consider the bistatic scattering from a sphere. The linear polarization rotation has been found, however it remains to find the RCS magnitude for the rotated polarization. It turns out that away from a forward scattering direction, the bistatic scattering RCS, σ, of a sphere is constant:

$$\sigma(\beta) = \pi\, a^2 \qquad (2.10)$$

where β is the bistatic angle and *a* is the radius of the circle (see Ruck, G., Barrick, D., Stuart, W. & Krichbaum, C., 1970, equation 3.2-25, page 156). Note that the non-forward scattering direction $0 <= \beta <= \pi-\delta$, where $\delta = O(1/(k\,a))$, where *k* is the wavenumber magnitude. The above RCS formula is in error by ~5% at $ka = 20$ and the error decreases rapidly for increasing *ka*.

It is assumed that for convex bodies other than a sphere, in the high frequency limit the RCS will be similar to that of the sphere, except that the RCS will be dependent upon the local radius, or radii of curvature. Furthermore, in a collection of 1cm gravel stones, it is noted that surfaces giving the brightest specular reflections over any area will be those with large radii of curvature, for example many times greater than 1cm, even when the stone diameter is 1cm on average.

In the example calculation that follows, to simplify the results the radius of curvature is taken to be $a=1/\sqrt{\pi}$, thus giving bistatic RCS $\sigma = 1$, except for in the forward scattering direction.

3. Bistatic Radar Geometry Model

In this section a representative example is set up with the transmitter at a grazing angle 45° pointing down at a specular scattering point at the origin, **S** = [0; 0; 0]. The transmitter is seen as the blue point in Figure 1, and the blue lines represent the polarization horizontal and vertical directions. The origin is shown in black. An example receiver position is shown in red with its polarization directions shown. The three black lines emanating from the origin point to the Transmitter, to the receiver, and along the bistatic vector which points along their mean. The polarization rotation resulting from the specular bistatic scattering is calculated via equation 2.4 to be 69° and is represented by the green lines at the receiver location.

For the fixed transmitter position described above where the grazing angle is 45°, the bistatic RCS results for scattering from a sphere with radius $1/\sqrt{\pi}$ across all directions in a direction datadome (the positive z hemisphere) are

shown in Figure 2. The upper image shows the linear co-polar and circular cross-polar result both equivalent under equation 2.9, and the lower image shows the linear cross-polar and circular co-polar result both equivalent under equation 2.9. The transmitter location is marked by a blue dot at Azimuth = 0° and Elevation = 45°, and the rest of each image shows bistatic polarized RCS as a function of receiver position.
Since the scattering model is in the physical optics regime, and the forward scattering point is far below this datadome hemisphere, it follows that these RCS values presented are accurate for metal spheres of radius $1/\sqrt{\pi}$ valid for wavelengths shorter than $1/(10\sqrt{\pi})$ or frequencies above $10c\sqrt{\pi}$, where c is the speed of light.

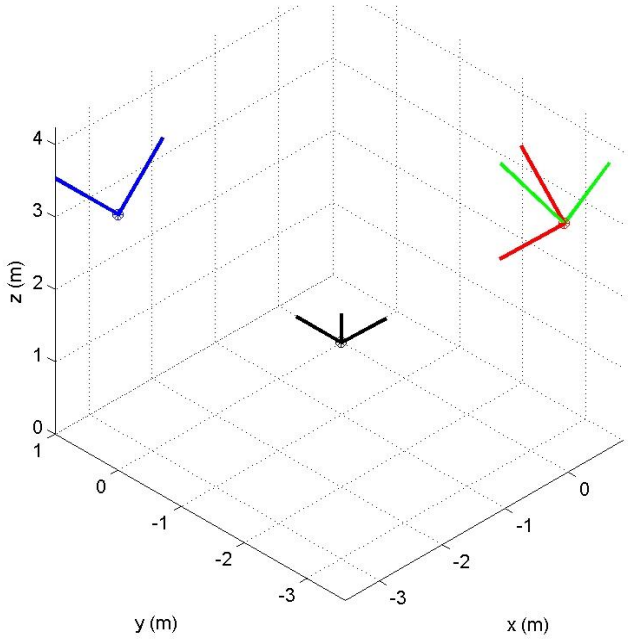

FIGURE 1. The bistatic scattering scene. The transmitter, receiver and scattering points are shown in blue, red and black respectively. The polarization rotation due to specular scattering is 69° and represented in green.

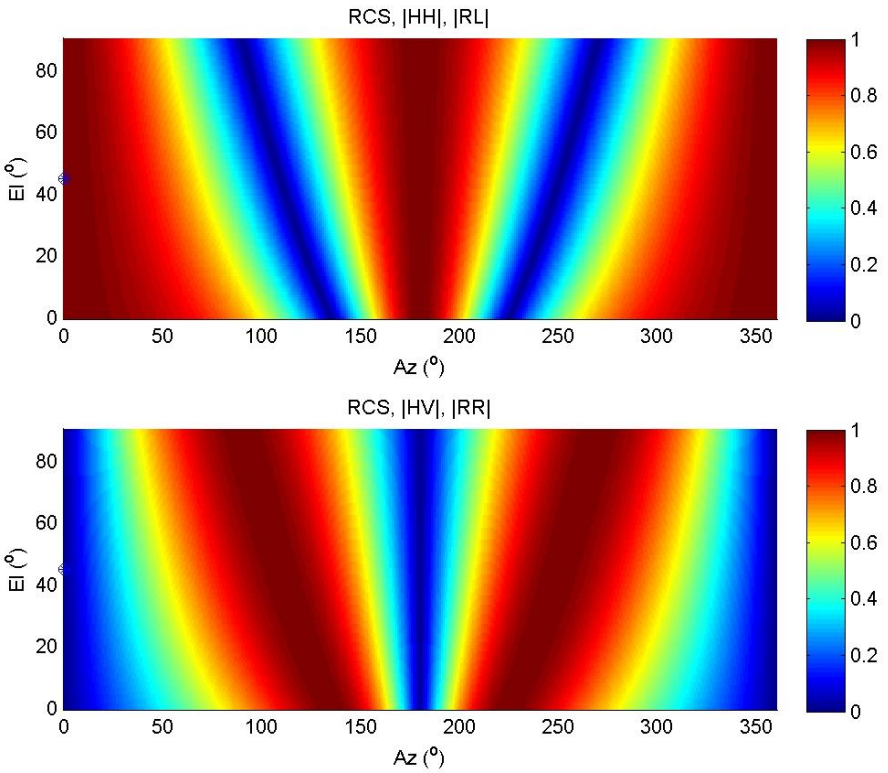

FIGURE 2. Bistatic RCS of a sphere in the physical optics regime showing linear and circular polarization basis combinations. The transmitter is located at azimuth = 0 and elevation = 45°, whereas the receiver is swept over the datadome hemisphere.

For improved visualisation, the data presented in Figure 2, can be rendered from a three-dimensional datadome representation as seen in Figure 3a for linear co-polar and circular co-polar, and in Figure 3b for linear cross-polar and circular co-polar, where the transmitter position is indicated by the blue dot and blue lines.

From the Figures 2 and 3 it can be seen that quasi monostatic scattering exhibits the polarimetric RCS similar to the monostatic backscattering case that one expects from a sphere, however for bistatic azimuth angles greater than 50° there is significant deviation. In Figure 4, graphs of bistatic RCS datadome cuts through the two polarimetric datadomes are presented. Figure 4a shows a receiver direction azimuth cut grazing angle fixed at 45°. On this graph the transmitter is located at 0° azimuth. It can be seen that the various basis co and cross-polar RCS values vary between 0 and 1 and are out of step with each other, so that when one is at a minimum, the other is at a maximum.

Figure 4b shows a grazing angle cut where the azimuth angle is fixed at 90°. Recall that the transmitter is located at azimuth = 0° and elevation angle = 45°. It can be seen that in this geometry, linear cross-polar bistatic RCS is larger than the co-polar value, except for when the receiver grazing angle is 0° where they are equal.

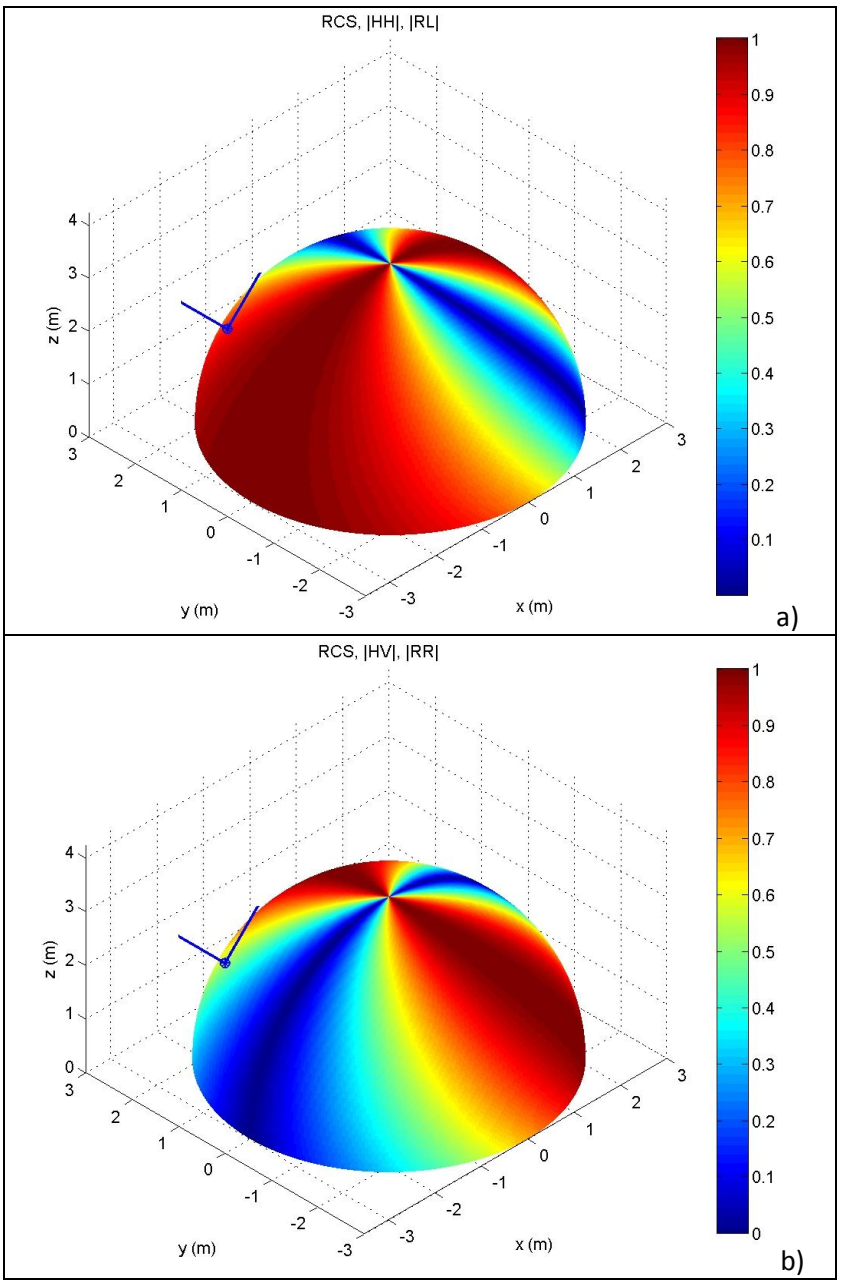

FIGURE 3. Receiver Bistatic RCS datadome of a sphere in the physical optics regime showing linear and circular polarization basis combinations. The transmitter is located at azimuth = 0° and elevation = 45°, whereas the receiver is swept over the datadome hemisphere.

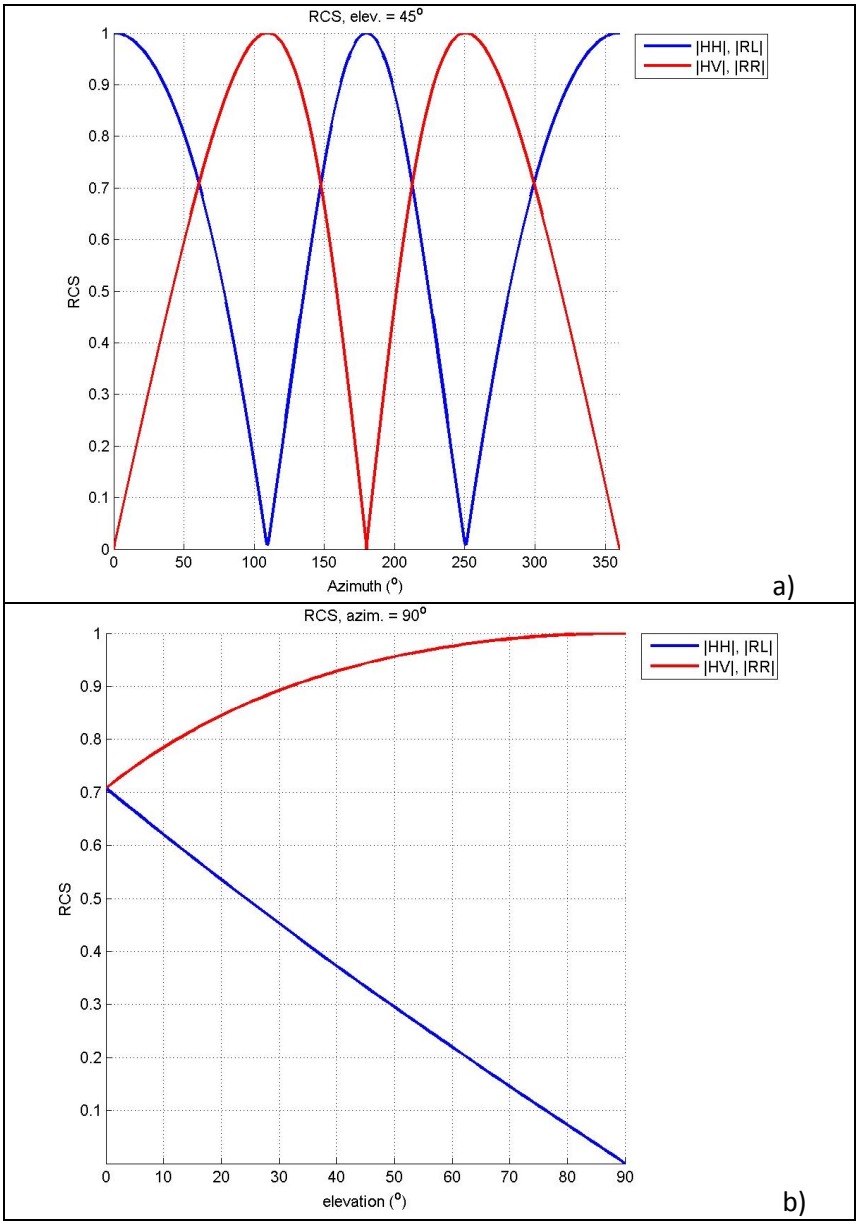

FIGURE 4. Graphs showing receiver azimuth or elevation cuts through the bistatic RCS polarization datadomes presented in Figures 2 and 3. (a) presents azimuth cuts where the elevation angle is fixed at 45°. (b) presents elevation cuts where the receiver azimuth angle is fixed at 90° (b). In both cases the transmitter position is fixed at 0° azimuth angle and 45° grazing angle.

4. Bistatic SAR coherence improvement through polarimetry

When it is the case that the diffuse specular scattering model is dominant over a given terrain, then it follows from the above that a given linear polarization rotation will maximise received RCS from a given specular scatterer at any point on the ground. In far-field-SAR therefore, one need only appropriately adjust the twist angle of the receiving antenna for each of the two bistatic SAR collections to maximise coherence between the collections, or apply the equivalent polarimetric decomposition in a fully polarimetric radar receiver.

In the near-field-SAR scenario however, interaction with each point on the ground will have its own optimal linear polarization rotation for maximum RCS because angles of incidence and specular reflection will vary significantly from place to place within the near-field-SAR illuminated scene. Hence a Spatially Variant Polarization (SVP) decomposition should be implemented for maximum RCS and coherence. Physically this may be achieved by utilising a dual polarization receiver and signal post processing.

Regarding the SAR image formation process, for far-field-SAR, one may apply the appropriate polarimetric decomposition post image formation through a simple complex linear addition of polarimetric images.

However for near-field-SAR, for example where the receiver is close-in to the scene, the situation will be more complicated. For example, in the back-projection algorithm, a spatially variant polarization rotation must be implemented when adding each range profile contribution to the image scene. Such a near-field-SAR scenario could be envisaged in the case of a spaceborne radar platform illuminating the Earth, and a static or close-in airborne bistatic receiver capturing scattered radar energy from a large illuminated footprint on the ground. The Pharos concept is an example of such a system (see Muff, D.G., Blacknell, D. & Nottingham, M.R., 2012).

5. Summary

It has been shown that when there is specular scattering resulting from any bistatic radar geometry, that a transmitted linear polarization will be affected in a non-trivial way, and for the case of specular diffuse scattering it is rotated in a well-defined way. Over a diffuse scattering scene, where scattering results from convex bodies spread throughout the scene, the specular diffuse scattering model presented may be dominant and robust over the whole scene. In situations where this diffuse scattering is dominant, when one seeks to maximise coherence between bistatic collections, then the scattered polarization rotation should be taken into account. It should therefore be the case that improved bistatic SAR coherence will be observed when the appropriate polarizations are applied specifically to each of the two bistatic geometry collections. In the near-field-SAR scenario, it follows that a spatially variant (per-pixel) polarimetric rotation should be applied to each bistatic SAR collection, likely as part of the actual image formation process, to capture the appropriate linear polarization rotation and therefore maximise coherence between two near-field-SAR collections. In the far-field-SAR scenario, the polarization decomposition reduces to a post image formation complex linear combination of bistatic SAR images.

Whilst the polarimetric effects from physical optics specular scattering have been investigated, it is noted that scattering of different types and in other physical scattering regimes may dominate in different circumstances. Similar calculations can be performed for scatterers in other physical scattering regimes, such as the Rayleigh “low frequency” regime, and in this situation, non-trivial well understood polarimetric effects are also present. However there may be circumstances where it may be difficult to model polarimetric scattering, and in these situations it would be appropriate to measure bistatic polarimetric scattering effects to determine an empirical scattering model.

In general, for different terrain, it may be that other spatially variant bistatic polarization decompositions may give rise to greater coherence or serve other utilities such as simply providing greater bistatic RCS (and therefore signal to noise ratio) or improved terrain characterization.

REFERENCES

Andre, D., Morrison, K. & Blacknell, D., 2013, “Spatially Variant Incoherence Trimming for Improved SAR CCD”, SPIE Defence Security and Sensing 2013

Andre, D., Morrison, K. & Blacknell, D., 2013, “Spatially Variant Incoherence Trimming for Improved Bistatic SAR CCD”, IEEE Radar Conference 2013

Blacknell, D, Andre, D & Finch, C., 2010, “SAR Coherent Change Detection (CCD) Over Mountainous Regions”, International conference on synthetic aperture sonar and synthetic aperture radar (SAS/SAR) 2010

Willis, N & Griffiths, H, 2007, “Advances in Bistatic Radar”, Scitech Publishing inc

Muff, D.G., Blacknell, D. & Nottingham, M.R., 2012, “Pharos – a SAR concept to accelerate advanced exploitation”, IET International Conference on Radar Systems 2012

Ruck, G., Barrick, D., Stuart, W. & Krichbaum, C., 1970, “Radar Cross Section Handbook, Vol. 1”, Plenum Press

Ulaby, F. & Elachi, C., 1990, “Radar Polarimetry for Geoscience Applications”, Artech House Inc.